NIP IMPINGED CENTER-WINDING INCLUDING A NONLINEAR BEAM MODEL

By

C. Mollamahmutoglu[1], J. K. Good[2], R. Markum[2], and J. W. Gale[3]
[1]Yildiz Technical University, TURKEY
[2]Oklahoma State University, USA
[3]Rockline Industries, USA

ABSTRACT

Nip pressure is commonly applied in winding processes in order to maintain structural stability and prevent air entrainment at high speeds. In nip induced winding modeling nip and roll are assumed to be beams with representative springs for the stiffness of the roll material between them [1], [2]. Depending on the application, typical rolls can measure up to more than 5 meters with different end constraints. Thus corresponding nip rolls, depending on the end constraints, and winding conditions can bend and rotate in such a way that linear beam theory can become inadequate especially in case of rolls which are wound from webs with length-wise persistent thickness variations. These bending deformations and/or different end conditions requires a geometrically nonlinear robust formulation which allows realistic engagement, disengagement and reengagement of a nip beam. In this study an axis-symmetric winding model, a roll compaction model and a nonlinear beam model coupled in order to simulate center-winding with a nip. Winding model calculates inner stresses and strains and updates the geometry and material properties with respect to incoming CMD tension profile. In the same time, as winding simulation continues, compaction model produces representative materially nonlinear radial stiffness coefficients for the wound roll in radial direction. These nonlinear springs, differing in height (in radial direction) are engaged by the representative nip beam in order to calculate the associated nip induced pressures along CMD on the wound roll. Finally these values in turn are used for calculation of the incoming tensions at various CMD locations for the winding model. The complete model uses an axisymmetric winding model [3] and a roll compaction model [4] previously developed by the lead author. The investigation and the integration of the nonlinear beam model for robust nip beam simulation under different end conditions is the original contribution of this study. Von Karman strains are assumed for the nip beam and a nonlinear finite element formulation is developed and integrated into the general algorithm. Effects of persistent web thickness variations and various end conditions, and usage of a nonlinear formulation vs. a linear formulation are studied as well.

INTRODUCTION

Nip application has various benefits in winding operations. Primary objectives are preventing air entrainment at high speed winding processes and maintaining structural stability. Also distributing the web line tension more uniformly through CMD thus maintaining a more uniform mechanical state (radial pressure distribution, uniformity at hoop tension) is desired as well. Especially for the webs which has CMD thickness variations (all webs have this to some extent as it is almost impossible to produce a perfectly flat uniform web) result in rolls with profiles which deviate from cylindrical shape considerably. As it is well known that the incoming web tension is distributed according to the roll profile, having a more uniform profile is crucial for a uniform tension allocation along CMD. As nip is engaging with the roll, it reduces the irregularity of the profile by pressing the ridges and results in an overall more regular profile. Nip also induces additional tension via friction mechanism. This "nip induced tension" (NIT) contributes to the incoming tension and results in a more compact, tight and robust roll structure. Briefly winding with a nip considerably alters the mechanical state of a wound roll.

In winding operations knowledge of the mechanical state and related defects is crucial for the industrial efficiency. In order to take preventive actions before winding a roll by trial and error, wound roll models have been developed throughout research activities. These theoretical models address the stress, strains and displacements inside rolls computationally and are strong alternatives for other costly trial methods. Modeling efforts started with 1D geometrical representation of a wound roll in the context of a plane stress/strain problem. One pioneering study assumed an orthotropic linear elastic model and attempted analytical solution [5]. Eventually nonlinear material behavior of the wound roll was addressed by Pfeiffer. [6]. He showed that radial modulus E_r was pressure dependent and can be characterized via fitting the experimental stress-strain curves with exponential functions. Based on this nonlinearity Hakiel developed a nonlinear numerical solution of plane strain approximation of a wound roll [7]. As typical roll includes thousands of layers and during winding mechanical properties changes it was required to solve the problem by adding layer over layer and updating the state of the material after every addition. 1D models could only address the radial and circumferential variables thus 2D axisymmetric models emerged which could produce results for CMD nonuniformities as well. [8, 9]. Early 2D models were obtained by combing nonlinear 1D models based on Hakiel's model as distinct sectors along CMD and parsing the incoming tension according to the current roll profile during winding. Hakiel and Cole verified their 2D model by comparing the core pressures from their model with experimental pressures obtained via a segmented instrumented core. Other than the mechanical or geometrical compatibility at the outer layer there were no continuity between 1D sectors. Thus these kind is collectively termed pseudo-2D models. State-of-art of winding models are the ones based on axisymmetric finite element representation of a wound roll. Each layer is represented via a series of quadrilateral finite elements connected at nodes thus structural continuity along CMD is maintained. Also quadrilateral elements can assume different side lengths which allows modeling nonuniform thickness variations along CMD as well. This real 2D modeling efforts started with uniform thickness assumptions and incorporation of incoming web tension as a uniform pressure loading at the outer surface of the roll via thin pressure vessel approximation of the outer hoop tension [10]. Later thickness variations were incorporated and tension allocation at the outer layer was addressed via multi-point constraints between the winding layer and the roll profile. [2] The one developed by the

lead author is the pinnacle of the axisymmetric winding models and utilizes the concept of relaxation radius originally developed by Cole and Hakiel in their pseudo-2D model where they used it for tension allocation across discontinuous 1D sectors. A pre-stress type formulation was developed and relaxation process of the winding layer over nonuniform roll profile automatically resulted in mechanically equilibrated tension allocation with CMD structural continuity. This method proved to be more efficient and natural than the earlier 2D models and by allowing the natural relaxation of the winding layer automatically incorporates tension loss of the outer layer as well [11, 12]. Hence webs with considerable compressibility can be accounted automatically without resorting sophisticated geometrically nonlinear formulations. [13]. This center-winding model is verified with comparison of the core pressures with the experimental core pressures obtained via a segmented instrumented core similar to the one developed by Hakiel and Cole. [3].

In terms of models with nip winding, 1D models simply incorporated the NIT as an addition to the incoming web line tension. Most of the time NIT can be calculated with a simple approximation based on Coulomb friction where NIT is simply taken as the multiplication of the nip pressure with the kinetic coefficient of friction. [14] showed the validity of this approximation by solving Hakiel's nonlinear 1D model by adjusting the outer boundary condition due to additional tension induced by nip and comparing the model results with the experimental results. Addition of NIT on to incoming tension collectively produces the wound on tension WOT. Hoffecker [2] used this approach in his 2D axisymmetric finite element model of a wound roll. Now instead of a single NIT a finite roll would have variable NIT across CMD. In order to find NIT of a CMD location precise geometry of the roll profile and the stiffness of the nip-roll contact should be calculated first. Hoffecker assumed a beam on elastic foundation approach and calculated the contact stiffness based on Hertzian model. Assuming Euler-Bernoulli type beam representations for nip and roll, he then utilized Lagrange's multipliers in order to enforce the Hertzian based contact stiffness between nip finite elements and the roll finite elements. Later it was shown that the contact stiffness between nip and roll is quite different than a Hertzian type. In their study [4], authors used a plane strain finite element formulation with nonlinear radial modulus of elasticity E_r and a dedicated contact algorithm in order to calculate the radial stiffness of a wound roll. Authors of this article also verified that a shear modulus of $G_{r\theta} \approx 2E_r$ yielded results which compared nicely with experiments. Also in another study authors modeled the Beloit rho-meter hardness tester. The dynamic contact between the striker of the tester and the roll is based on the stiffness model. Again their stiffness model compared nicely with the experimental results. [15] Finally, in the realm of nip impinged 2D models, the lead author combined the pre-stress axisymmetric wound roll model and the stiffness model with a contact algorithm [1]. The contact model includes same Euler-Bernoulli type beam elements both for nip and roll but instead of Hertzian approach the stiffness is calculated from the dedicated stiffness model and the contact between nip and roll is enforced via penalty constraints. This model is verified on the segmented instrumented core by winding a PET web which was intentionally produced with thickness CMD variations. Thickness variations are measured with a beta-gage head which moves along CMD as the web passes beneath. Combination of the head's CMD velocity with web's MD velocity produced a zig-zag thickness data pattern which is then feed into the combined model. Winding model calculates inner stresses and strains and updates the geometry and material properties with respect to incoming CMD tension profile (WOT) and the thickness data provided. Then for each CMD sector of the axisymmetric roll, stiffness model produces representative materially nonlinear radial stiffness coefficients for the contact between

the roll and the nip beams. In the contact model, these nonlinear springs, differing in height (in radial direction) are engaged by the nip beam in order to calculate the associated nip induced pressures along CMD on the wound roll. Finally nip induced pressures are used for calculation of the NIT and thus WOT at various CMD sectors for the winding model and this completes the cycle.

In this study the combined model in [1] will be presented with an improved contact algorithm which incorporates geometrically nonlinear beam elements based on von Karman strains. Moreover depending on the stiffness conditions and roll profile new contact algorithm allows for engagement, disengagement and reengagement of the springs. Effects of various boundary conditions for the nip and roll beams will be investigated. Results will be verified based on new measurements of thickness variation. We begin by presenting the components of the combined model, first the winding model and then the stiffness model. These will be presented briefly as they are dedicated studies concerning them in the literature by authors. Here we added them for the sake of completeness. The contact model is presented in detail.

THE AXISYMMETRIC WINDING MODEL

Winding model is responsible from solving for the entire stress and strain state within a roll while it is being wound from web. It solves for each model layer and incrementally updates the displacements (geometry), stresses and strains. This layer-wise approach is not only due to the nature of the problem, but also due to nonlinearity of radial modulus of elasticity E_r. One of the most common used form of nonlinear representations is due to Pfeiffer [6] with two material parameters K_1 and K_2:

$$E_r = K_2(K_1 - \sigma_{rr}) \qquad \{1\}$$

Here σ_{rr} is the radial stress. Standard finite element formulation of axisymmetric bodies are well known and we will not repeat it. Also the detailed model can be found in [3]. Here emphasis is given to the incorporation of the incremental loading to due addition of a new layer. Figure 1 is showing the addition of a typical new layer, consisting of M elements, with thickness variation which caused the non-cylindrical roll profile. In center winding simulations the shape of the roll profile is the sole responsible for the tensions allocated through CMD locations (sectors). We utilized the notion of relaxation radius and define a pre-stress based on the amount of strain defined with respect to relaxation radius.

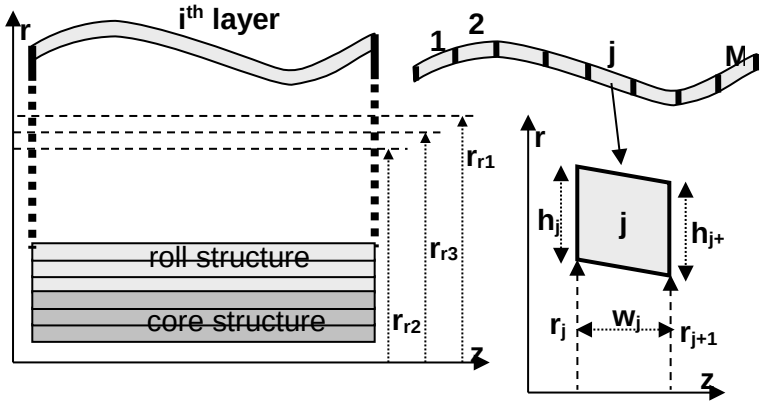

Figure 1 – Axisymmetric Winding Model, Thickness Variation, Sector and Quadrilateral Elements

Pre-stress Formulation

Pre-stress formulation begins with the definition of the load vector for j_{th} axisymmetric element in i_{th} layer which can be given as:

$$F_e = -2\pi \int B^t \sigma_{0,j} r dr dz \qquad \{2\}$$

Here B is the usual strain displacement matrix for axisymmetric case and $\sigma_{0,j}$ is the pre-stress vector for the j[th] element and defined with the tangential modulus of elasticity E_θ:

$$\sigma_{0,j} = \left[0\ 0\ 0\ E_\theta \frac{r_{ave,j} - r_r}{r_r}\right]^t \qquad \{3\}$$

where $r_{ave,j}$ is the average radial position of the element and relaxation radius r_r is obtained from the mechanical equilibrium of the outer layer with the definition; the radial position assumed by a stress free layer:

$$r_r = \frac{E_\theta \sum_{j=1}^{M} r_{ave,j} h_{ave,j}}{(E_\theta + T_W) \sum_{j=1}^{M} h_{ave,j}} \qquad \{4\}$$

In $\{4\}$ $h_{ave,j}$is the average thickness for the element. When $\{3\}$ is used in $\{2\}$ with $\{4\}$, an element load vector is obtained. Then the usual assembly procedure is carried out and the system for the current state can be solved for incremental displacements by considering the current state of E_r is kept constant.

$$K^i \Delta U^i = F^i \qquad \{5\}$$

In $\{5\}$ K^i is the global axisymmetric stiffness matrix written for the state when solving for the i[th] layer. It is obtained by the assemblage of the regular axisymmetric finite elements but the material matrix used in the construction includes current values of associated E_r terms. Similarly F^i is the assembled load vector which uses $\{2\}$ for the elements of the winding layer i. Thus solution vector corresponds to the incremental displacements ΔU^i. After solution incremental stresses are calculated as in the usual finite

element procedure and the radial stresses are updated. These in turn are used for the state update by the calculation of new E_r values for each element inside the current roll. This type of linearization is adequate and yields acceptable results considering that usual wound roll is consisting of hundreds of model layers.

Effect of Nip Induced Tension

When center-winding with nip is considered nip induced tensions across CMD for the winding layer i should also be taken into account. We simply adopted the solution based on Coulomb type frictional approach proposed by Good et al [14] and modify the pre-stress formulation of jth element by changing the pre-stress vector {3} according to associated nip induced pressure NIT_j:

$$\sigma_{0,j} = \left[0\ 0\ 0\ E_\theta \frac{r_{ave,j} - r_r}{r_r}\right]^t + NIT_j \qquad \{6\}$$

and NIT_j is calculated with the amount of nip pressure Pj exerted on the sector for the existing roll profile, roll stiffness and nip load:

$$NIT_j = \mu_k \frac{P_j}{w\, h_{real}} \qquad \{7\}$$

Here μ_k is the kinetic coefficient of friction and w is the width of the sector. Notice that h_{real} is the real web thickness and not the model thickness used in the winding model. Nip ınduced pressures Pj for j=1,2,.. M will be determined by the contact model as will be explained in contact section.

THE STIFFNESS MODEL

In order to calculate the nip induced pressures across CMD a contact algorithm is used. Sectors are represented as nonlinear springs which provides the radial stiffness between the nip and roll. Stiffness model is responsible for obtaining the characteristics of these nonlinear springs. For this purpose each sector is modeled as a 2D plane strain problem under contact with a cylinder representing the nip. This pressing cylinder can be taken as rigid or can be modeled as covered with an elastic layer. Figure-2 shows the general configuration of the stiffness problem. At some instance winding model stops and passes information to the stiffness model. This information includes the current radius of sectors, and current state of the elements. Stiffness model maps this material information on a refined 2D mesh and conducts a nonlinear compression analysis where the state is updated as compression occurs. An important point here is the effect of the in-plane shear modulus $G_{r\theta}$. Authors found this parameter is also state dependent and taking $G_{r\theta} = 2E_r$ produces results which compares well with experimental results for very different class of material. Details of the related algorithms and experimental verification can be found in the study by authors [4]. Finally a discrete load-displacement data is obtained and it is seen that a second order function can be fitted to obtain the nonlinear spring response for a given level of deformation. Stiffness calculations are carried out for all sectors $j=1,2,..,M$ and set of spring parameters (α_j, β_j) are obtained:

$$f_{sj} = \alpha_j \delta_{cj}^2 + \beta_j \delta_{cj} \qquad \{8\}$$

In {8} f_{sj} is the spring force when the spring compaction (deformation) is δ_{cj}. Now it is understood that $Pj = fsj$ in {7} when δ_{cj} assumes the equilibrium compaction values for the

contact between nip and roll for a given level of nip load and roll profile. This will be covered in contact model below where nip and roll are represented as beams with these nonlinear springs each has a height depending on the current average sector it represents.

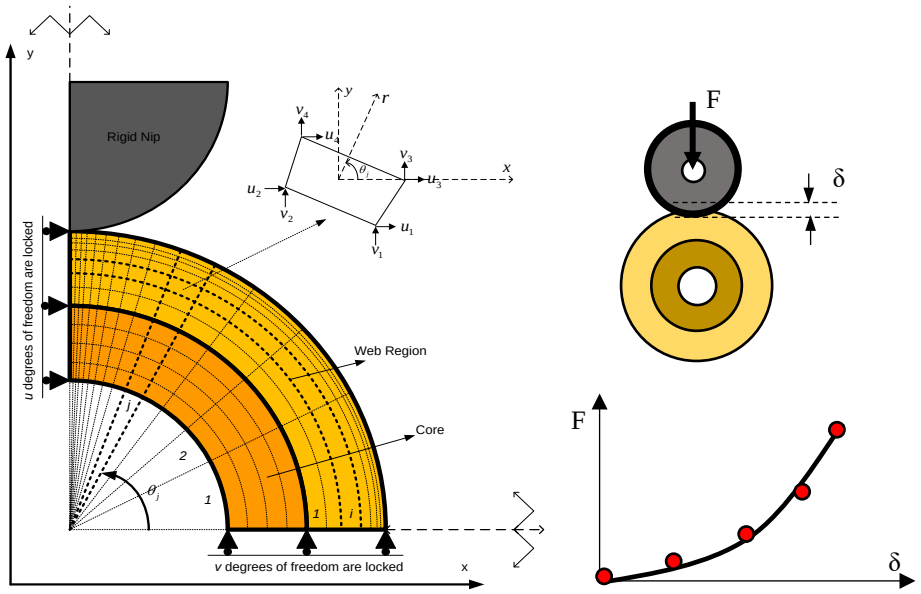

Figure 2 – Stiffness Model Based on 2D Nonlinear Elastic Model and Extracting Spring Parameters

Hardness Testing

In another study [15] authors developed a simple analytical method which calculates hardness (based on Beloit Rho-meter) of a roll when the α, β is provided by the stiffness model. Thus when the center-winding model is used hardness values across CMD can also be easily determined as stiffness model is already in use and (α_j, β_j) are readily obtained for all sectors. This will enhance the prediction capabilities of the combined model as it is another form of information besides stress and displacements which can be readily used in the quality assessment. Details can be found in the mentioned study. Here we briefly give information for the sake of completeness. Rho values are scaled deceleration values when the striker head impacts the roll surface. Assuming the system is elastic during impact then conservation of energy requires:

striker_spring_elastic_energy@initial_position =

striker_spring_elastic_energy@max_depth + roll_elastic_energy@max_depth

Selected positions for the striker head are zero velocity positions so there are only elastic potentials. If we define max depth the striker head attains (that is also the position for max Rhos) as δ_{max} then we can write down the energy equation as:

$$\frac{1}{2}k_s{x_{in}}^2 = \frac{1}{2}k_s(x_{gap} + \delta_{max})^2 + E_{roll}(\delta_{max}) \quad \{9\}$$

where $E_{roll}(\delta)$ is the elastic energy stored in the roll spring, x_{in} is the height spring rises above free state and x_{gap} is the spring travels below free state. Since roll spring is nonlinear $E_{roll}(\delta)$ can be calculated with the integration of the force deformation relation {8}:

$$E_{roll}(\delta) = \int_0^{\delta} F(\delta)d\delta \rightarrow E_{roll}(\delta_{max}) = \frac{\alpha {\delta_{max}}^3}{3} + \frac{\beta {\delta_{max}}^2}{2} \quad \{10\}$$

Substituting {10} into {9} we will obtain a third order polynomial equation of δ_{max}:

$${\delta_{max}}^3 + \frac{3(\beta+k_s)}{2\alpha}{\delta_{max}}^2 + \frac{3k_s x_{gap}}{\alpha}\delta_{max} + \frac{3k_s}{2\alpha}\left(x_{gap}^2 - x_{in}^2\right) = 0 \quad \{11\}$$

Nonlinear equation {11} can be easily solved with one of the root finding methods like Newton-Raphson. After the solution, newly found δ_{max} can be immediately used for calculating Rho_{max} i.e. Rho value for the maximum deceleration which in turn can be calculated from the maximum spring force $F(\delta_{max})$ divided with the striker head's mass m_s:

$$Rho_{max} = \frac{F(\delta_{max})}{(3.76\ g\ m_s)} \quad \{12\}$$

Here 3.76 appeared as the scaling parameter as 3.76 g = 1 Rho.

THE NONLINEAR CONTACT MODEL

Contact model is responsible to resolve the amount of pressure applied to different sectors depending on the current roll profile and nip load. We need to go through a nonlinear beam model based on von Karman strains. We introduce an engaging, disengaging and reengaging algorithm implemented via the nonlinear beam model. Because of the uneven roll profile contact problem includes geometrical nonlinearity because of nonlinear beam model and contact nonlinearity because of the ever changing contact conditions.

Von Karman Beam

Euler-Bernoulli beam model assumes that after the bending the cross-sections remain plane and perpendicular to the beam axis (elastic curve). The displacement field reads:

$$u(x,z) = u_0(x) - z{w_0}'(x) \quad \{13.a\}$$

$$v \equiv 0 \quad \{13.b\}$$

$$w(x) = w_0(x) \quad \{13.c\}$$

where u,v,w are the displacements of a point along x,y,z directions respectively and $'$ represents first derivation with respect to x. The usual infinitesimal strain-displacement relations produces the well-known linear strain components with the only non-zero component along x direction ε_{xx} :

$$\varepsilon_{xx} = u_0' - z{w_0}''(x) \quad \{14\}$$

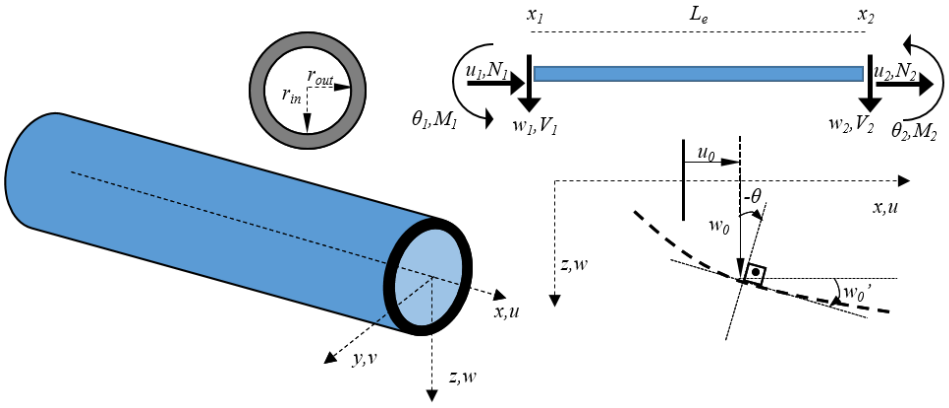

Figure – 3 von Karman Beam Model

Here $''$ represents second derivation with respect to *x*. Also $w_0' = -\theta$ since positive values for the slope of the elastic curve results in negative rotations around *y* axis. Von Karman assumes that as the rotations of the beam are getting bigger, contribution of higher order terms related with them should be included. According to this assumption the complete strain-displacement relations with nonlinear terms included results in:

$$\varepsilon_{xx} = u_0' - zw_0'' + \frac{{w_0'}^2}{2} \qquad \{15\}$$

The higher order term is nothing but the square of the rotations ${w_0}'$ of the beam's sections. Material is assumed to be elastic with the Young's Modulus of *E*. Thus corresponding stress nonzero component σ_{xx} is given as:

$$\sigma_{xx} = E\varepsilon_{xx} \qquad \{16\}$$

Now a finite element model can be developed by utilization of the virtual work principle, which states that the internal virtual work done by the stresses is equal to the external virtual work done by the external forces:

$$\delta W_{int} = \delta W_{ext} \qquad \{17\}$$

Here δ indicates a virtual variation of the associated symbol. We denote the nodal displacements and external force vector of a beam element by *U* and *F* respectively:

$$U = [u_1\ w_1\ \theta_1\ u_2\ w_2\ \theta_2]^t \qquad \{18.a\}$$

$$F = [N_1\ V_1\ M_1\ N_2\ V_2\ M_2]^t \qquad \{18.b\}$$

In the absence of distributed and body loads virtual work expression {17} can be given as:

$$\int \sigma_{xx}\delta\varepsilon_{xx}dV = \delta U^t F \qquad \{19\}$$

where δ represents a variation of the associated variable:

$$\delta\varepsilon_{xx} = \delta u_0' - z\delta w_0'' + w_0'\delta w_0' \quad \{20\}$$

$$\delta U = [\delta u_1\ \delta w_1\ \delta\theta_1\ \delta u_2\ \delta w_2\ \delta\theta_2]^t \quad \{21\}$$

After substituting the virtual work expressions of the variables {20}, {21} into the virtual work expression {19}, also assuming the coordinate system is passing through the centroid of the hollow cross section and constant material and geometric properties we obtain:

$$\int \sigma_{xx}\delta\varepsilon_{xx}dV = EA\int_{x_1}^{x_2}\delta u_0'\left(u_0' + \frac{{w_0'}^2}{2}\right)dx + EA\int_{x_1}^{x_2}\delta w_0' w_0'\left(u_0' + \frac{{w_0'}^2}{2}\right)dx + EI\int_{x_1}^{x_2}\delta w_0'' w_0''dx \quad \{22\}$$

$$\delta U^t F = \delta u_1 N_1 + \delta u_2 N_2 + \delta w_1 V_1 + \delta w_2 V_2 + \delta\theta_1 M_1 + \delta\theta_2 M_2 \quad \{23\}$$

Here A is the area and I is the second moment of inertia of the cross section with respect to the centroid:

$$A = \pi({r_{out}}^2 - {r_{in}}^2),\ I = \frac{\pi({r_{out}}^4 - {r_{in}}^4)}{4}$$

Usual finite element approximation functions for a typical two node element can used:

$$u_0(x) = \sum_{i=1}^{2} u_i\phi_i(x)\ ,\ w_0(x) = \sum_{i=1}^{2} w_i\psi_i(x) + \sum_{i=1}^{2}\theta_i\chi_i(x) \quad \{24.a,b\}$$

$$\delta u_0(x) = \sum_{i=1}^{2}\delta u_i\phi_i(x),\ \delta w_0(x) = \sum_{i=1}^{2}\delta w_i\psi_i(x) + \sum_{i=1}^{2}\delta\theta_i\chi_i(x) \quad \{25.a,b\}$$

Here ϕ_i are linear shape functions and ψ_i, $\chi_i$are Hermite type shape functions of a regular Euler-Bernoulli beam element. Unlike the linear finite elements now the displacement field is a quadratic function of the displacements variables thus virtual work results in a cubic relation. Hence the nonlinearity arises. One way of linearization is using some rotation terms w_0' as known variables from some previous iteration of the general solution. After substituting the finite element approximations {24.a,b}, {25.a,b} into the virtual work expressions {22}, {23}, invoking {19} we arrive at:

$$\delta u_i\left\{EA\int_{x_1}^{x_2}{\phi'}_i{\phi'}_j dx u_j + \frac{EA}{2}\int_{x_1}^{x_2} w_0'{\phi'}_i{\psi'}_j dx w_j + \frac{EA}{2}\int_{x_1}^{x_2} w_0'{\phi'}_i{\chi'}_j dx\theta_j - N_i\right\} = 0 \quad \{26\}$$

$$\delta w_i\left\{EA\int_{x_1}^{x_2} w_0'{\psi'}_i{\phi'}_j dx u_j + (\frac{EA}{2}\int_{x_1}^{x_2}{w_0'}^2{\psi'}_i{\psi'}_j dx + EI\int_{x_1}^{x_2}{\psi''}_i{\psi''}_j dx)w_j + (\frac{EA}{2}\int_{x_1}^{x_2}{w_0'}^2{\psi'}_i{\chi'}_j dx + EI\int_{x_1}^{x_2}{\psi''}_i{\chi''}_j dx)\theta_j - V_i\right\} = 0 \quad \{27\}$$

$$\delta\theta_i\left\{EA\int_{x_1}^{x_2} w_0'{\chi'}_i{\phi'}_j dx u_j + (\frac{EA}{2}\int_{x_1}^{x_2}{w_0'}^2{\chi'}_i{\psi'}_j dx + EI\int_{x_1}^{x_2}{\chi''}_i{\psi''}_j dx)w_j + (\frac{EA}{2}\int_{x_1}^{x_2}{w_0'}^2{\chi'}_i{\chi'}_j dx + EI\int_{x_1}^{x_2}{\chi''}_i{\chi''}_j dx)\theta_j - M_i\right\}=0 \quad \{28\}$$

Utilization of arbitrariness of the virtual displacements results in the usual element finite element equations for an element *e*:

$$K_e(U_e)U_e = F_e \qquad \{29\}$$

As noticed element stiffness matrix is not independent from the nodal displacements, since it is including w_0' terms:

$$w_0'(x) = \sum_{i=1}^{2} w_i \psi'_i(x) + \sum_{i=1}^{2} \theta_i \chi'_i(x) \qquad \{30\}$$

Hence is a function of w_i and θ_i nodal displacements. Also, it is understood that the stiffness matrix not symmetric for this particular way of linearization; leaving w_0' as a known value from a previous iteration. In fact, stiffness matrix can be given as a summation of a linear part and nonlinear part:

$$K_e(U_e) = {K_e}^L + {K_e}^{NL} \qquad \{31\}$$

where ${K_e}^L$ is the regular linear stiffness matrix of Euler-Bernoulli beam finite element:

$${K_e}^L = \begin{bmatrix} \frac{EA}{L_e} & 0 & 0 & -\frac{EA}{L_e} & 0 & 0 \\ 0 & \frac{12EI}{{L_e}^3} & -\frac{6EI}{{L_e}^2} & 0 & -\frac{12EI}{{L_e}^3} & -\frac{6EI}{{L_e}^2} \\ 0 & -\frac{6EI}{{L_e}^2} & \frac{4EI}{L_e} & 0 & \frac{6EI}{{L_e}^2} & \frac{2EI}{L_e} \\ -\frac{EA}{L_e} & 0 & 0 & \frac{EA}{L_e} & 0 & 0 \\ 0 & -\frac{12EI}{{L_e}^3} & \frac{6EI}{{L_e}^2} & 0 & \frac{12EI}{{L_e}^3} & \frac{6EI}{{L_e}^2} \\ 0 & -\frac{6EI}{{L_e}^2} & \frac{2EI}{L_e} & 0 & \frac{6EI}{{L_e}^2} & \frac{4EI}{L_e} \end{bmatrix} \qquad \{32\}$$

Linear part is exactly integrated but an exact (full) integration of the nonlinear part ${K_e}^{NL}$ is subjected to the fact that membrane strains inside the beam should be allowed to vanish when there is not any axial loading:

$$u_0' + \frac{{w_0'}^2}{2} \approx 0 \qquad \{33\}$$

But this is not possible with full integration of all terms as ϕ_i used for the approximation of $u_0(x)$ are linear functions whereas ψ_i and χ_i used for the approximation of $w_0(x)$ are Hermit type and cubic. Thus while $u_0'(x)$ is represented with a constant throughout beam axis, ${w_0'}^2$(x) is represented with a quartic function and membrane condition cannot be satisfied and there will be some fictitious membrane strains which will cause unrealistic increase in the associated stiffness terms. Increased stiffness will result in stiffer behavior hence the phenomenon "membrane locking" will occur. A solution for this problem is using reduced integration for the terms including $w_0(x)$ in membrane strains. One point Gauss Quadrature will result in a constant assumption automatically and will allow membrane strains to assume zero when required depending on the boundary and loading conditions. One point Gauss Quadrature is simply using the mid-point, $x_m = (x_1 + x_2)/2$, value for a function *f*, and

$$\int_{x_1}^{x_2} f dx \approx f(x_m) L_e \quad \{34\}$$

Now the nonlinear part can be given as:

$$K_e{}^{NL} = \begin{bmatrix} 0 & \frac{3EA}{4L_e}w_0' & -\frac{EA}{8}w_0' & 0 & -\frac{3EA}{4L_e}w_0' & -\frac{EA}{8}w_0' \\ \frac{3EA}{2L_e}w_0' & \frac{9EA}{8L_e}w_0'^2 & -\frac{3EA}{16}w_0'^2 & -\frac{3EA}{2L_e}w_0' & -\frac{9EA}{8L_e}w_0'^2 & -\frac{3EA}{16}w_0'^2 \\ -\frac{EA}{4}w_0' & -\frac{3EA}{16}w_0'^2 & \frac{EAL_e}{32}w_0'^2 & \frac{EA}{4}w_0' & \frac{3EA}{16}w_0'^2 & \frac{EAL_e}{32}w_0'^2 \\ 0 & -\frac{3EA}{4L_e}w_0' & \frac{EA}{8}w_0' & 0 & \frac{3EA}{4L_e}w_0' & \frac{EA}{8}w_0' \\ -\frac{3EA}{2L_e}w_0' & -\frac{9EA}{8L_e}w_0'^2 & \frac{3EA}{16}w_0'^2 & \frac{3EA}{2L_e}w_0' & \frac{9EA}{8L_e}w_0'^2 & \frac{3EA}{16}w_0'^2 \\ -\frac{EA}{4}w_0' & -\frac{3EA}{16}w_0'^2 & \frac{EAL_e}{32}w_0'^2 & \frac{EA}{4}w_0' & \frac{3EA}{16}w_0'^2 & \frac{EAL_e}{32}w_0'^2 \end{bmatrix} \quad \{35\}$$

where $w_0' = \frac{3(w_2 - w_1)}{2L_e} + \frac{\theta_1 + \theta_2}{4}$. The usual assembly procedure can be applied and the system equations can be obtained:

$$K(U)U = F \quad \{36\}$$

where *K*, *U* and *F* are global stiffness matrix, displacement vector and load vector respectively. *K(U)* is used to indicate that stiffness matrix is function of the nodal displacements due to nonlinear part. Clearly this is a set of nonlinear equations and requires iteration for solution. One way of solution of {36} is to utilize direct substitution method due to Pickard:

$$K(U^{k-1})U^k = F \quad \{37\}$$

Here k is the iteration counter with *k=1,2,..* and U^k is the solution for the kth iteration. So at the beginning a U^0 should be provided and this is generally taken as the zero vector, i.e. $U^0=0$. Now at every iteration the norm of difference between the new displacement vector and the old displacement vector is calculated and divided with the norm of the current displacement vector in order to obtain a measure for the relative error:

$$E^R = \frac{\|U^k - U^{k-1}\|}{\|U^k\|} \quad \{38\}$$

Iterations are stopped and the current displacement vector is assumed to be the solution for a given load vector *F* when the relative error becomes smaller than a predetermined tolerance value ϵ_{tol}:

$$E^R < \epsilon_{tol} \rightarrow U \cong U^k \quad \{39\}$$

Generally $\epsilon_{tol} = 0.001$ yields acceptable results. Most of the time Pickard's method faces with difficulties for convergence when the nonlinearity is getting stronger thus not the whole part of a new iteration is used, instead only a portion of it:

$$U^k = \rho U^k + (1 - \rho)U^{k-1} \quad \{40\}$$

Here $1 \geq \rho > 0$ and obviously $\rho = 1$ resumes the original case. This will increase the number of iterations considerably and even sometimes the method completely fails no matter the value of ρ is selected. Thus we are opting to use a more robust approach: Newton-Raphson method. We define a residual vector *R* which depends on the displacement vector *U*:

$$R(U) = K(U)U - F \quad \{41\}$$

Now we can expand *R(U)* into a Taylor series around a known or assumed U^0 and retain only on linear terms:

$$R(U) \approx R(U^0) + \left.\frac{dR}{dU}\right|_{U=U^0} (U - U^0) \quad \{42\}$$

Now for the exact U^* solution we would have from $R(U^*)=0$:

$$\left.\frac{dR}{dU}\right|_{U=U^0} (U^* - U^0) = -R(U^0) \quad \{43\}$$

But since we have only retained on linear terms and ignored the rest, this attempt will only give an iteration towards real solution and U^* should be replaced with a U^1:

$$\left.\frac{dR}{dU}\right|_{U=U^0} (U^1 - U^0) = -R(U^0) \quad \{44\}$$

Denoting the difference between the consecutive displacement vectors in the iteration at the k^{th} step, as the incremental displacement vector ΔU^k, and the derivative of the residual vector with respect to displacements with the so called tangent stiffness matrix as T^{k-1} we arrive at the Newton-Raphson iteration sequence for $k=1,2,..$:

$$T^{k-1}\Delta U^k = F - K^{k-1}U^{k-1} \quad \{45\}$$

where *k-1* indicates that the associated terms are calculated with the U^{k-1}

$$T^{k-1} = \left.\frac{dR}{dU}\right|_{U=U^{k-1}}, K^{k-1} = K(U^{k-1}) \quad \{46\}$$

And the explicit form of the tangent stiffness matrix is:

$$T = \frac{dK}{dU}U + K \quad \{47\}$$

Carrying out the necessary derivations and taking into account reduced integration for membrane locking, components of the *T* matrix can be given:

$$T_e = \begin{bmatrix} 0 & \frac{3EA}{2L_e}w_0' & -\frac{EA}{4}w_0' & 0 & -\frac{3EA}{2L_e}w_0' & -\frac{EA}{4}w_0' \\ \frac{3EA}{2L_e}w_0' & \frac{9EA}{4L_e}\Omega & -\frac{3EA}{8}\Omega & -\frac{3EA}{2L_e}w_0' & -\frac{9EA}{4L_e}\Omega & -\frac{3EA}{8}\Omega \\ -\frac{EA}{4}w_0' & -\frac{3EA}{8}\Omega & \frac{EAL_e}{16}\Omega & \frac{EA}{4}w_0' & \frac{3EA}{8}\Omega & \frac{EAL_e}{16}\Omega \\ 0 & -\frac{3EA}{2L_e}w_0' & \frac{EA}{4}w_0' & 0 & \frac{3EA}{2L_e}w_0' & \frac{EA}{4}w_0' \\ -\frac{3EA}{2L_e}w_0' & -\frac{9EA}{4L_e}{w_0'}^2 & \frac{3EA}{8}\Omega & \frac{3EA}{2L_e}w_0' & \frac{9EA}{4L_e}\Omega & \frac{3EA}{8}\Omega \\ -\frac{EA}{4}w_0' & -\frac{3EA}{8}\Omega & \frac{EAL_e}{16}\Omega & \frac{EA}{4}w_0' & \frac{3EA}{8}\Omega & \frac{EAL_e}{16}\Omega \end{bmatrix} \quad \{48\}$$

Here $\Omega = u_0' + \frac{3{w_0'}^2}{2}$ and explicitly calculated at the center of an element as:

$$\Omega = \frac{u_2 - u_1}{L_e} + \frac{3}{2}\left(\frac{3(w_2 - w_1)}{2L_e} + \frac{\theta_1 + \theta_2}{4}\right)^2$$

Now for a given initial displacement vector the iteration can commence and as in direct iteration can be stopped when the relative error drops below a predetermined threshold value:

$$E^R = \frac{\|\Delta U^k\|}{\|U^k\|},\ E^R < \epsilon_{tol} \rightarrow U \cong U^k \quad \{49\}$$

As in the Pickard's method we can introduce a convergence parameter just like ρ but Newton-Raphson method is much more robust and generally does not need such adjustments, though it is more expensive in terms of one iteration cycle, because we need to calculate the tangent stiffness matrix. In fact in most cases the load vector *F* is not applied as a whole, since it can be too large to lead a converged solution, but rather in a stepwise manner. So assuming we have *N* steps for the loading and total load is divided into equal portions for each steps then for s^{th} load step we need to solve for *s=1,2,..*:

$$T^{k-1}{}_s \Delta U^k{}_s = F_s - K^{k-1}{}_s U^{k-1}{}_s \quad \{50\}$$

$$F_s = \frac{s}{n}F, \text{ and } U^0{}_s = U^{k^*}{}_{s-1}$$

Here k^* is the last iteration for the solution of $(s\text{-}1)^{th}$ load step and obviously $U^{k^*}{}_0 = 0$ as we start the solution with the zero vector at the beginning. After convergence check is satisfied at a load step the solution proceeds to the next load step with the starting displacement vector equal to the final displacement vector of the previous load step. When *s=n* is completed total *F* is applied. Now we can solve some examples and compare the results with commercial code which utilizes sophisticated nonlinear beam models and also with the simple linear solutions from strength of materials: a simple supported beam (length *L*, bending stiffness *EI*) with a concentrated load (*P*) applied at the middle of the span. Dimensionless graph shows the results from linear theory and the nonlinear theory together. As the PL^2/EI is getting bigger, linear theory predicts larger deformations. This result is true for a pinned-pinned type constraint, i.e. edges are constrained in axial direction. Otherwise von Karman beam predicts the same displacements. This is because von Karman theory models the effect of axial force on the bending rotations, i.e. the stiffening effect of axial force. It is not a true nonlinear theory

which takes the deformed and undeformed states separately into account. But it is quite satisfactory when the edges of a beam is constrained in axial directions. Fortunately this is the case for the nip and roll beams. Deflection results for $PL^2/EI=2$ are also given for linear, von Karman nonlinear and exact nonlinear theory from a commercial finite element package. It is seen that performance is remarkably satisfactory.

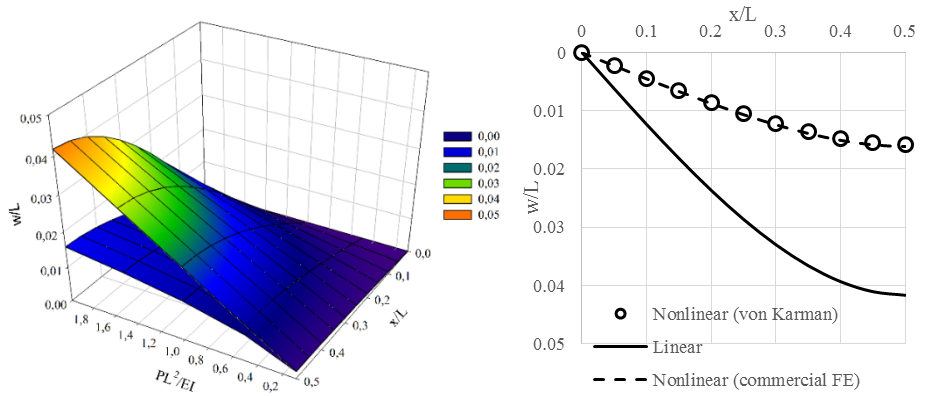

Figure 4 – von Karman Beam vs. Linear Beam

Nonlinear Contact Algorithm

As indicated before contact algorithm is based on the beam representations of the nip and roll separately. The radial stiffness between them is obtained via the stiffness model. As the stiffness model performs analysis sector by sector, it produces F-δ relations for each sector depending on the current state of the roll. These nonlinear springs are quadratic functions of indentation displacement as seen before. In contact analysis their relative heights are also important as these will dictate the ever changing geometrical conditions of the contact as the nip engages the roll. Spring heights are directly obtained from the winding model as it keeps track of the roll profile after addition of every lap. For a winding model with M number of sectors, we used $2M$ elements both for nip and roll beam. So every sector is represented with 2 beam elements. The mesh of the nip and roll beams match so that the contact occurs at the nodes all the time as seen from the figure.

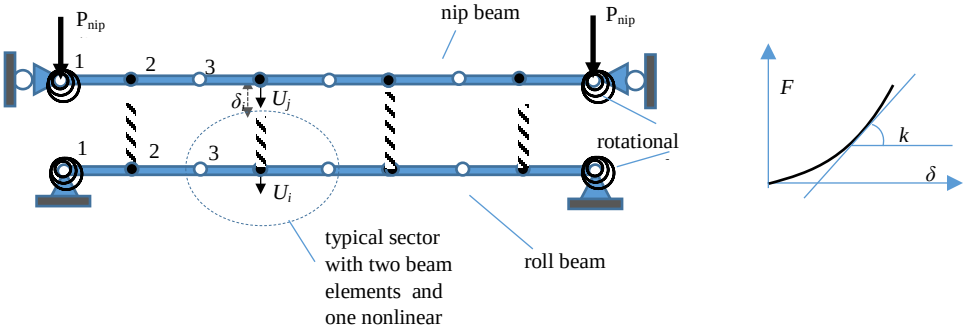

Figure 5 – The Contact Model with Roll and Nip Beam Representations and Nonlinear Springs

The nonlinear equations for the roll and nip beam are separately obtained and then combined within a general frame. The augmented (due to constraints and spring interactions) general system is given as:

$$\begin{bmatrix} \bar{T}_{roll} & C \\ C^t & \bar{T}_{nip} \end{bmatrix}^{k-1} \begin{bmatrix} \Delta U_{roll} \\ \Delta U_{nip} \end{bmatrix}^{k} = \begin{bmatrix} 0 \\ F_{nip} \end{bmatrix} + \begin{bmatrix} \bar{F}_{roll} \\ \bar{F}_{nip} \end{bmatrix} + \begin{bmatrix} F_{sp} \\ -F_{sp} \end{bmatrix} - \begin{bmatrix} \bar{K}_{roll} & 0 \\ 0 & \bar{K}_{nip} \end{bmatrix}^{k-1} \begin{bmatrix} U_{roll} \\ U_{nip} \end{bmatrix}^{k-1} \quad \{51\}$$

or implicitly as:

$$\bar{T}^{k-1}\Delta U^{k} = \bar{F} - \bar{K}^{k-1}U^{k-1} \quad \{52\}$$

Here $\bar{T}_{roll}, \bar{T}_{nip}, \bar{K}_{roll}, \bar{K}_{nip}, U_{roll}, U_{nip}, \Delta U_{roll}, \Delta U_{nip}$ are the augmented tangent stiffness matrices, augmented stiffness matrices, displacement vectors and incremental displacement vectors for roll and nip respectively. They are written for *3(M+1)* degrees of freedoms. F_{nip} is the force vector including the current level of the nip load:

$$F_{nip} = [0 \quad P_{nip}/2 \quad 0 \quad \cdots \quad 0 \quad P_{nip}/2 \quad 0]^t \quad \{53\}$$

C is the constraint matrix which enforces the contact boundary conditions between nip and roll beams which includes current values of the nonlinear spring stiffness terms of the active springs. A linear geometrical constraint of a general type between to typical degrees of freedom (U_i and U_j) on one of the beams can be given as:

$$c_i U_i - c_j U_j = c_0 \quad \{54\}$$

Then a corresponding energy is added to the system potential with the penalty constraint Υ :

$$\frac{\Upsilon}{2}(c_i U_i - c_j U_j - \mathrm{c}_0)^2 \quad \{55\}$$

Invoking the virtual work results in additional terms for stiffness matrix and the force vector:

$$\bar{K}_{ii} = K_{ii} + \Upsilon \mathrm{c}_i{}^2, \bar{K}_{jj} = K_{jj} + \Upsilon \mathrm{c}_j{}^2, \bar{K}_{ij} = K_{ij} - \Upsilon \mathrm{c}_i \mathrm{c}_j, \bar{K}_{ji} = K_{ji} - \Upsilon \mathrm{c}_i \mathrm{c}_j, \quad \{56\}$$

$$\bar{F}_i = F_i + \Upsilon \mathrm{c}_i \mathrm{c}_0, \bar{F}_j = F_j - \Upsilon \mathrm{c}_j \mathrm{c}_0$$

In the linearization process these terms directly will be carried into the tangent stiffness matrix as they are added to the linear part of the stiffness matrix and symmetry of tangent stiffness matrix is still preserved:

$$\bar{T}_{ii} = T_{ii} + \Upsilon \mathrm{c}_i{}^2, \bar{T}_{jj} = T_{jj} + \Upsilon \mathrm{c}_j{}^2, \bar{T}_{ji} = \bar{T}_{ij} = T_{ij} - \Upsilon \mathrm{c}_i \mathrm{c}_j \quad \{57\}$$

Now if degree of freedom of a beam, e.g. U_i, is fully restrained then $c_i=1$, $c_j=c_0=0$ and Υ is set to a large number, i.e. *1E10*Max[*K_{ii}*]*. If U_i and U_j are locked together (for example enforcing equal displacements for nip beam's ends) then $c_i=c_j=1$, $c_0=0$ and again Υ is set

to a large number. If there is a linear spring, like the rotational springs at the ends of beams with a corresponding degrees of freedom then $c_i=1$, $c_j=c_0=0$ and $\Upsilon=k_r$, where k_r is the rotational stiffness of the spring. Treatment of the nonlinear springs requires special attention as they are not always in contact, and can engage, disengage and reengage. Assume that a spring which is connected to a i^{th} degree of freedom of the roll beam is corresponding to a j^{th} degree of freedom of the nip beam then the potential of the spring can be given as:

$$\Upsilon\left(\frac{\alpha\left(c_iU_i-c_jU_j-\mathrm{c}_0\right)^3}{3}+\frac{\beta\left(c_iU_i-c_jU_j-\mathrm{c}_0\right)^2}{2}\right) \qquad \{58\}$$

Carrying out the virtual work procedure results in additional terms in equilibrium for these corresponding degrees of freedom:

$$F_{sp,i}=-\Upsilon c_i\left(\alpha\left(c_iU_i-c_jU_j-\mathrm{c}_0\right)^2+\beta\left(c_iU_i-c_jU_j-\mathrm{c}_0\right)\right) \qquad \{59.a\}$$

$$F_{sp,j}=\Upsilon c_j\left(\alpha\left(c_iU_i-c_jU_j-\mathrm{c}_0\right)^2+\beta\left(c_iU_i-c_jU_j-\mathrm{c}_0\right)\right) \qquad \{59.b\}$$

and linearization leads additional terms for the tangent stiffness matrix:

$$\bar{T}_{ii}=T_{ii}+\Upsilon\mathrm{c}_i{}^2\left(2\alpha\left(c_iU_i-c_jU_j-\mathrm{c}_0\right)+\beta\right) \qquad \{60.a\}$$

$$\bar{T}_{jj}=T_{jj}+\Upsilon\mathrm{c}_j{}^2\left(2\alpha\left(c_iU_i-c_jU_j-\mathrm{c}_0\right)+\beta\right) \qquad \{60.b\}$$

$$\bar{T}_{ij}=T_{ij}-\Upsilon\mathrm{c}_i\mathrm{c}_j\left(2\alpha\left(c_iU_i-c_jU_j-\mathrm{c}_0\right)+\beta\right) \qquad \{60.c\}$$

Now setting $c_i=c_j=-1$, c_0 equal to negative of the initial gap distance between the roll and nip for the associated spring which connects i and j degrees of freedoms i.e. $c_0=-\delta_{ij}{}^0$ and taking $\Upsilon=1$ when $U_j-U_i+\delta_{ij}{}^0>0$ and $\Upsilon=0$ otherwise will engage the spring when it is compressed and disengage when it is freed. In fact $U_j-U_i+\delta_{ij}{}^0$ is nothing but the amount of spring deformation (compression taken as positive), $2\alpha\left(U_j-U_i+\delta_{ij}{}^0\right)+\beta$ is the current spring stiffness for that amount of compression and finally f_{sp} is the current value of corresponding spring force acting on the roll (f_{sp}) and nip ($-f_{sp}$):

$$f_{sp}=\left(\alpha\left(U_j-U_i+\delta_{ij}{}^0\right)^2+\beta\left(U_j-U_i+\delta_{ij}{}^0\right)\right) \qquad \{61\}$$

The node numbering is same for roll and nip beam so i^{th} degree of freedom of roll beam which corresponds to a j^{th} degree of freedom of nip beam has the relation $j=i+3(M+1)$ between them. But we also know that $(3M+1)$ is the size of sub-matrices of the general system so if NDOF=$(3M+1)$ then following can be written in terms of sub-matrices:

$$\bar{T}_{roll,ii}=T_{roll,ii}+\Upsilon\left(2\alpha\left(U_{NDOF+i}-U_i+\delta_i{}^0\right)+\beta\right) \qquad \{62.a\}$$

$$\bar{T}_{nip,ii}=T_{nip,ii}+\Upsilon\left(2\alpha\left(U_{NDOF+i}-U_i+\delta_i{}^0\right)+\beta\right) \qquad \{62.b\}$$

$$C_{ii}=-\Upsilon\left(2\alpha\left(U_{NDOF+i}-U_i+\delta_i{}^0\right)+\beta\right) \qquad \{62.c\}$$

$$F_{sp,i} = \Upsilon\left(\alpha\left(U_{NDOF+i} - U_i + {\delta_i}^0\right)^2 + \beta\left(U_{NDOF+i} - U_i + {\delta_i}^0\right)\right) \qquad \{62.d\}$$

Here ${\delta_i}^0$ is the initial gap for the spring which corresponds to the U_i degree of freedom of roll beam. This completes the nonlinear formulation of the roll-nip beam system with the geometrical boundary conditions, rotational springs, locked vertical movement of nip ends, and engaging ($\Upsilon=1$), disengaging ($\Upsilon=0$) nonlinear springs. The general algorithm of the solution is given below. Algorithm is based on displacement controlled unless all the springs are under contact and activated. If contact occurs for all springs it will switch to force a controlled solution and applies the remaining load in increments. For the displacement controlled section a tolerance number ϵ is used to determine the contact whether a spring is engaging or disengaging. When a gap size is closer to zero (from negative or positive side) than $1/\epsilon_\delta$ of the initial maximum gap size it is considered engaged. $\epsilon_\delta=0.01$ gives satisfactory contact resolution.

α_i,βi	i[th] spring parameters
ϵ_δ	contact tolerance parameter
δ_i	i[th] spring's current gap
δ_i^0	i[th] inital gap size
$\delta_{min}{}^0$	initial min. gap size
δ_{min}	current minimum gap
δ_{tol}	contact tolerance
δ_{ci}	i[th] spring's compaction
Υ_i	i[th] spring's lock parameter
Fnip	nip load
Ftot	current total load on nip
F	current load for load step iteration
h_i	i[th] spring height: i[th] sector's radius
h_{max}	maximum spring height
k_{stot}	current total spring stiffness
k_{si}	i[th] spring's current stiffness
N	total number of load steps
s	load step iterator
STATUS	configuration parameter checking for full contact

Table 1 – Contact Algorithm Key

1-gather initial data
*roll profile; spring heights (h_i) (from the winding model)
*sector α_i and β_i coefficients for nonlinear springs (from the stiffness model)
*material and geometrical properties, boundary conditions for nip and roll beams (inner outer radii, Young's moduli etc.)

2-prepare for contact
*position the nip beam at h_{max} and determine initial gap sizes δ_i^0 for all springs (sectors) $\delta_i^0 = h_{max}-h_i$

	*determine initial min gap size δ_{min}^0 and set the contact tolerance $\delta_{tol}=\epsilon_\delta*\delta_{min}^0$	
	*determine the contact status and set the locks for all springs if $\delta_i^0<\delta_{tol}$ then $\Upsilon_i=1$ else $\Upsilon_i=0$ STATUS=$\Sigma\Upsilon_i$	
	*set total load to zero $F_{tot}=0$, set compactions to zero for all springs $\delta_{ci}=0$, set current minimum gap to initial $\delta_{min}=\delta_{min}^0$, set gap sizes to initial gap sizes $\delta_i=\delta_i^0$	
	3-engage nip	
	Do while ($F_{tot}<F_{nip}$)	main cycle
	findt the current total spring stiffness k_{stot} for the engaged springs if $\Upsilon_i=1$, $k_{si}=2\alpha_i\delta_{ci}+\beta_i$, $k_{stot}=\Sigma k_{si}$	main cycle
	*find the amount of the load to apply and adjust if necessary if $STATUS=M$ then $F=F_{nip}-F_{tot}$ else $F=k_{stot}*\delta_{min}/2$ if $F+F_{tot}>F_{nip}$ then $F=F_{nip}-F_{tot}$	main cycle
	*solve the system for F in N load steps: Do $s=1,N$ start convergence iterations for the load step s:	incremental load cycle
iteration cycle	Do while ($E^R<\epsilon_{tol}$) (load is scaled $s*F/N$) applied load $F_{tot}+s*F/N$	incremental load cycle
iteration cycle	setup nonlinear system of equations, tangent stiffness matrix, stiffness matrix etc., and apply geometric boundary conditions and other related constraints like rotational springs etc.	incremental load cycle
iteration cycle	add the associated terms to the system for activate springs ($\Upsilon_i=1$)	incremental load cycle
iteration cycle	solve for incremental displacements ΔU	incremental load cycle
iteration cycle	update the displacement vector $U=U+\Delta U$	incremental load cycle
iteration cycle	update gap sizes $\delta_i=\delta_i^0+U_i-U_{i+3(M+1)}$ just engaged: if $\lvert\delta_i\rvert<\delta_{tol}$ then $\Upsilon_i=1$ and $\delta_{ci}=0$ disengaged: else if $\delta_i>\delta_{tol}$ then $\Upsilon_i=0$ and $\delta ci=0$ already engaged: else if $\delta_i<-\delta_{tol}$ then $\Upsilon_i=1$ and $\delta_{ci}=\delta_{ci}+\Delta U_{i+3(M+1)}-\Delta U_i$	incremental load cycle
iteration cycle	calculate the relative error E^R for this iteration cycle	incremental load cycle
	update the status STATUS= $\Sigma\Upsilon_i$	main cycle
	find a new value for the minimum gap δ_{min} between disengaged springs ($\Upsilon_i=0$)	main cycle
	calculate current level of spring forces for active springs if $\Upsilon_i=1$ then $f_{si}=\alpha_i\delta_{ci}^2+\beta_i\delta_{ci}$ calculate current total force on the nip $F_{tot}=\Sigma f_{si}$	main cycle

RESULT: calculate the nip induced tensions for sectors as in {7} with $P_i=f_{si}$, $NIT_i=\mu*P_i/(h_{real}*w)$
w is the width for the sector, h_{real} is the real web thickness.

Table 2 – Nonlinear Contact Algorithm

THE CENTER-WINDING WITH NIP MODEL

The model is obtained by combining three models as indicated before. Figure 6 explains the cyclic interactions. As there is not enough material to compress and a prominent roll profile to engage and resolve various NIT, a predetermined amount of layers are wound with constant NIT. After this number of initial web layers are wound, throughout operations of winding model, stiffness and contact models are triggered and

called at certain number of additional layers as they are wound. When experiencing with a 1400 thousand layer model, which is wound with a web intentionally produced with MD-CMD thickness variations, it was observed that calling at every 50 layers produces satisfactory results with acceptable computational run times. For different webs, nip loads and winding conditions some runs maybe required to see the needed frequency of the calls for convergence

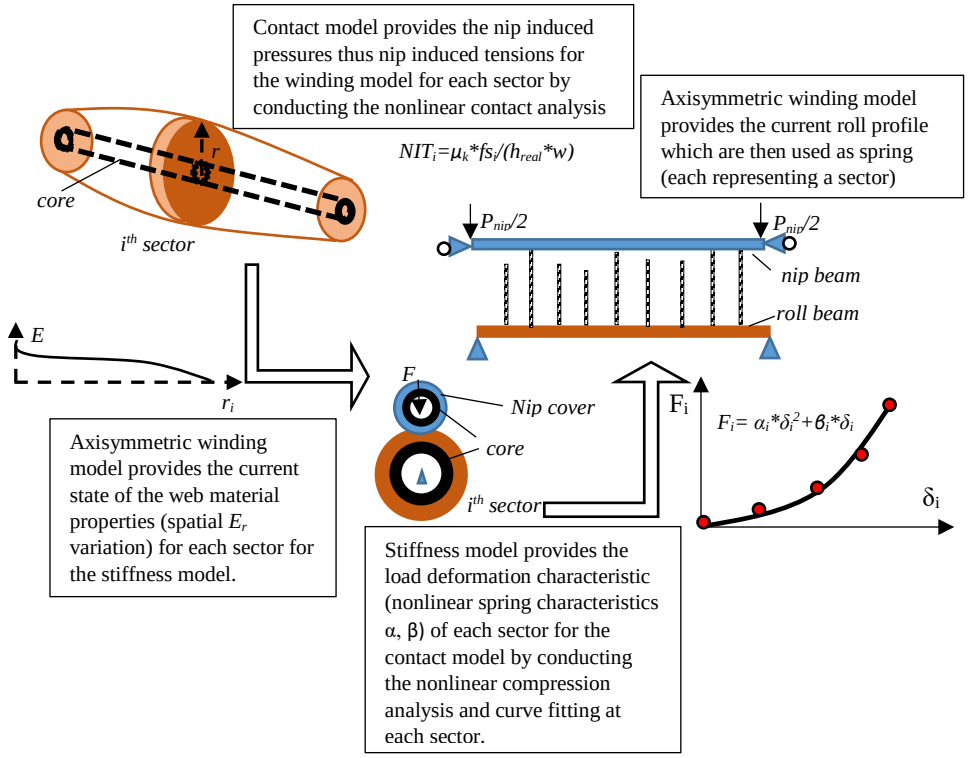

Figure 6 – The Combined Model Representative Cycle

RESULTS AND DISCUSSIONS

Experiments were carried out in WHRC for a polyester material which was intentionally produced with thickness variation. The roll tested is 61 cm wide and was cut from a 349 cm wide master roll. It has an average thickness of 76 µm and has both MD and CMD thickness variations. The model was run with both variations taken into account with a 2D thickness array. The spatial thickness data is obtained through set of experiments which made use of a noncontact ultrasonic method. The test roll is thought to be consisting of 24 equally wide CMD sectors and device head was positioned and kept stationary at each one of the CMD locations one by one while the web was moving in MD direction. Thus mapping MD variations through each one of the CMD sectors produced the 2D thickness data. A total of 1200 meters of web was measured which corresponds to a pile height of 10.16 cm on a 10.16 cm radius core. Measured full thickness data and its sector-wise average can be seen in Figure 7.

Verification

Core pressure measurements conducted on a specially designed and built segmented instrumented core which is consisting of independently movable aluminum rings. Rings are identical and each has a CMD width of 2.54 cm and 10.16 cm outer radius. The model was adjusted so that this type of core stiffness could be accounted for. Also hardness readings were taken with a Beloit Rho-meter after winding up to 10.16 cm pile height was completed. Hardness measurements were conducted on the same CMD locations as were the thickness measurements.

K_1(Kpa)	K_2	E_z, E_θ (MPa)	web v_{zr}, $v_{\theta r}$	web $v_{z\theta}$	avg. Thick. (μm)	width (cm)
0.01	290	4999	0.3	0.3	76	61
roll inner rad. (cm)	roll out. Rad. (cm)	core inner rad. (cm)	E_{core} (Gpa)	core v_{zr}, $v_{\theta r}$, $v_{z\theta}$	T_w (Mpa)	P_{nip} (Mpa)
10.16	20.32	9.5	69	0.33	2.3 & 3.45	2.3

Table 4 – Polyester Test Roll Properties

Table-4 includes the geometrical and material data for the tests. Both center-winding with nip and without nip was carried out. Two web line tensions of 2.3 Mpa and 3.45 Mpa were used and when nip was present a 2.3 Mpa of average nip load was applied for all cases. $\mu_k=0.3$ was used as kinetic coefficient of friction in the model between nip roll and the web.

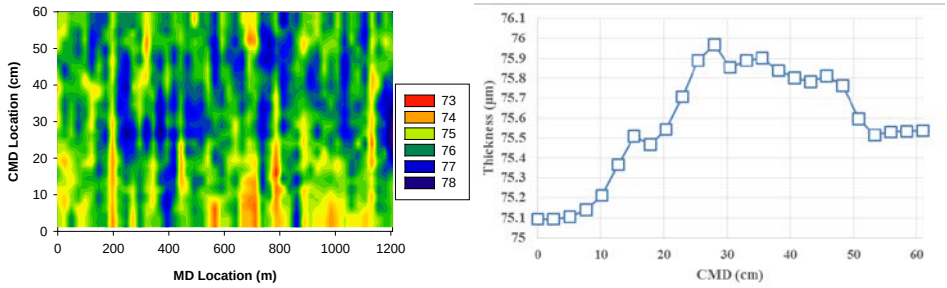

Figure 7 – Polyester Test Roll CMD/MD Full Thickness Variation and Average Thickness Variation

Figure 8 includes without a nip hardness measurements (rhos) and the model hardness results obtained via the hardness sub-model described previously. Figure 9 again includes the hardness comparisons between tests and model but this time a nip load of 2.3 Mpa was applied. Figure 10 includes the core pressure result comparisons for the case of Figure 8 and finally Figure 11 includes again core pressure comparisons of the case of Figure 9. It is seen that both hardness readings and core pressure readings are captured reasonably well with the combined model. This verification includes an inner and outer measurement as the core pressures are local around core region where as hardness readings are mostly related with the outer section of the roll as found by authors [15]. Thus model prediction capability can be assumed to be valid for the entire roll provided that enough thickness data is used. [3]

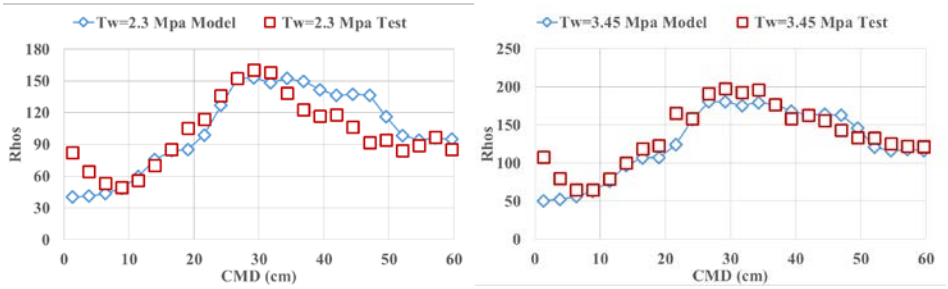

Figure 8 – Hardness Test and Model Comparisons for Center-winding w/o Nip

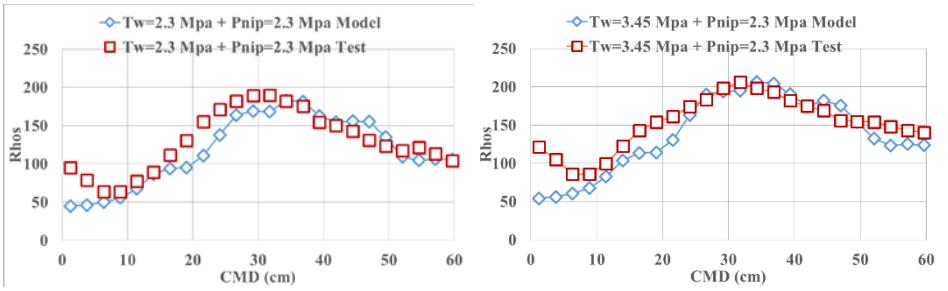

Figure 9 – Hardness Test and Model Comparisons for Center-winding w/ Nip

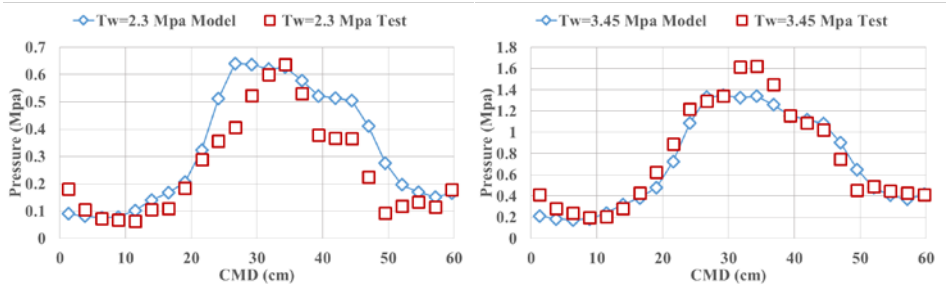

Figure 10 – Core Pressure Test and Model Comparisons for Center-winding w/o Nip

In the model runs we have assumed simple supported beam conditions both for nip and roll beams. In fact in case of a span length of 61 cm and an aluminum nip roll which has a radius of 20.32 cm, nip beam almost acted as a rigid beam. No difference was observed between a fixed-fixed type constrain and simple-simple type constraint. Also the constraint that the nip beam's ends are locked together for vertical movement did not play a significant role for this stocky nip beam. Various changes can be seen if the beam becomes slender and these cases are investigated with the model on some fictitious cases.

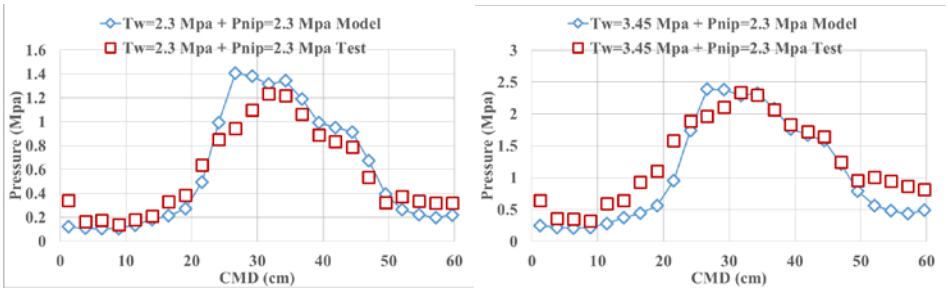

Figure- 11 Core Pressure Test and Model Comparisons for Center-winding w/ Nip

Effect of Nonlinearity and Boundary Conditions

In case of short (stocky) rolls both nonlinearity and boundary conditions do not seem to be effective. As the rolls become longer, end constraints and large deformations can change the nature of engagement of the nip beam. Also the robustness of the nonlinear algorithm comes into prominence. In order to show these effects we will use a hypothetical case which includes thickness variations. The roll we have tested was cut from a master roll. We will use the entire data of the master roll in order to produce the hypothetical roll for this section. The master roll was about 360 cm wide, hypothetical roll will be 940 cm wide. Thickness variation of the master roll will be stretched along the 960 cm length. T_w*=2.3 Mpa* and *Pnip=4.6 Mpa* is used. All other relevant material and geometrical data is exactly the same with the actual case. Nip beam is assumed to be made of aluminum with a radius of 10 cm and thickness of a 1cm. Figure 12 shows the thickness of the actual data and the sampled data with respect to data#. 24 sectors are used. The linear algorithm employs the regular linear stiffness matrix K^L and does not iterate for a given load step. Otherwise the main algorithm is the same as the nonlinear one. It also allows engagement, disengagement and reengagement but robustness is not the same. One of the constraints we used so far is the vertical constraint between the left and right ends of the nip beam. It enforces that both ends have the same amount of displacement, in other words it is trying to keep the nip horizontal. Another constraint we tested was the rotational springs attached to ends of the roll and nip beams. Two extreme cases are considered, simple support (k_r*=0*) and fixed ($k_r=\infty$), by setting the rotational stiffness value 0 or a large number (i.e. penalty constraint). k_r seems to be the least effective of all; all the different cases simulated over k_r gave almost same results. It only added to the stability of the linear algorithm as it helped prevent rigid body motions.

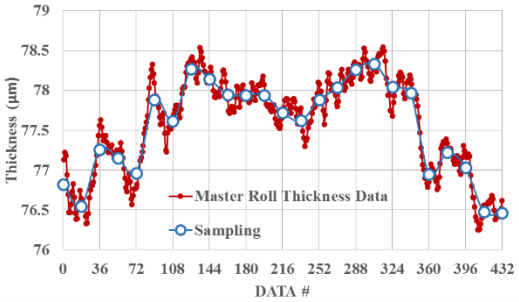

Figure 12 – Hypothetical Roll Thickness Data

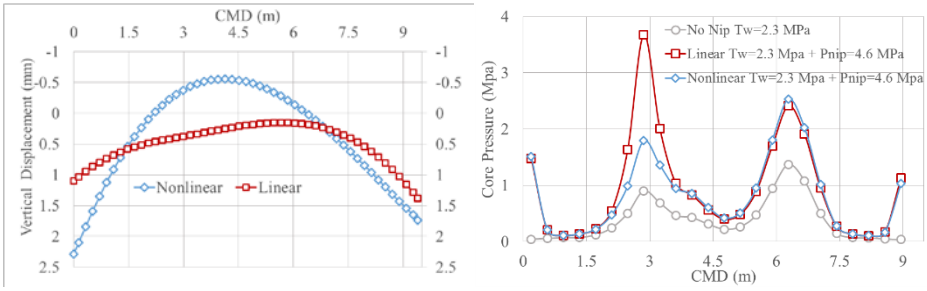

Figure 13 – Core Pressure and Nip Elastic Curve for Final Roll Profile Nonlinear vs Linear

Figure 12 shows results for the robustness of the nonlinear algorithm. When rigid body rotations are prevented by adding a small amount of rotational stiffness linear model approached nonlinear model. So the difference seen here is about the stability of the algorithm. In fact von Karman beam couples the axial strains with rotations and includes the stiffening effect coming from a tensioned member, so it predicts smaller displacements under same conditions.

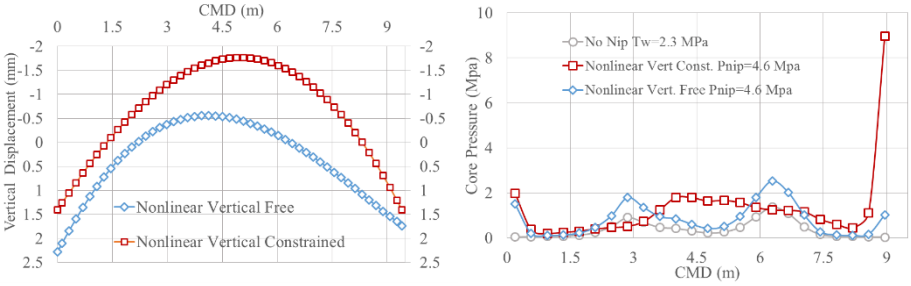

Figure 14 – Core Pressure and Nip Elastic Curve for Final Roll Profile, Nonlinear, Free vs. Cons. Vert. Disp.

Figure 14 shows the results for freeing the vertical locking constraint between nip ends. As seen from Figure 14 results at the edges are greatly affected. As the nip ends can displace independently it can engage both ends more equally depending on the respective stiffness values of the nonlinear edge springs. Figure 15 compares nonlinear and linear cases for ends constrained situation. This case is produced by using a smaller diameter for the nip in order to exaggerate nonlinear effects. Nip radius is selected as 8 cm and thickness as 0.8 cm. As expected linear theory predicts greater deformations but overall core pressures are very close to each other. In fact during the initial state of winding first 50 layers are wound with equal NIT as explained before, and core pressures are already characterized by this part. Also as seen from the nip profiles, after active NIT allocation starts, most of the time roll center is not engaged (negative deformations=nip is lifted). Thus difference is only becomes visible at the edges for this selected case.

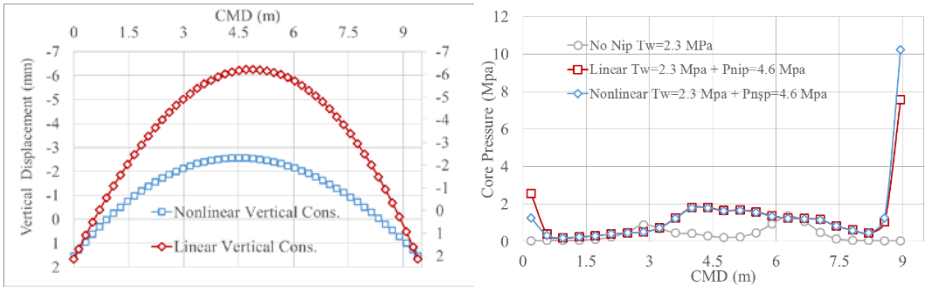

Figure 15 – Core Pressure and Nip Elastic Curve for Slender Profile Nonlinear vs Linear, Constrained Ends

CONCLUSIONS

A robust nonlinear nip engagement model is developed and integrated into an axisymmetric winding model. The combined model successfully captures the inner (core pressure verification) and outer (hardness verification) mechanical state of roll in case of center-winding with a nip. It is seen that end condition which locks the nip beam's vertical end displacements has the most effect on nip profile and roll engagement thus tension allocation. Other end condition which is related with the tilting stiffness of the ball bearings seem to be little of importance. Nonlinear model predicts deformations realistically by incorporating the stiffening effect of the axial stresses inside nip beam. Although the difference between nonlinear and linear models in terms of displacements were not that influential on the results of the selected examples there can be situations (slender nips, high nip loads, radical thickness variations) which are inadaptable with linear theory. Also cases where a nip is lifted or not, or when deformations of a nip are required; these can be addressed much more realistically. More research is needed to address the boundaries of linear and nonlinear theory in terms of effect of deformations but nonlinear theory is almost always superior in terms of numerical stability and this is something that should not be underestimated.

REFERENCES

1. Mollamahmutoglu, C., "A 2D Axis-symmetric Wound Roll Model Including Nip Effects," PhD Dissertation, Oklahoma State University, 2009.
2. Hoffecker, P., "The Analysis of a Nip Impinged, Three Dimensional Wound Roll," PhD Dissertation, Oklahoma State University, 2006.
3. Good, J. K., Mollamahmutoglu, C., Markum, R., and Gale, J. W., "Residual Winding Stresses Due to Spatial Web Thickness Variation," Transactions of ASME, Journal of Manufacturing Sci. and Eng., Vol. 139, Issue 3.
4. Mollamahmutoglu, C., Ganapathi, S., and Good, J. K., "Pressures on Webs in Wound Rolls due to Winding and Contact," Tappi Journal, Vol. 13, 2014, pp. 41-50.
5. Altmann, H. C., "Formulas for Computing the Stresses in Center-Wound Roll," Tappi Journal, Vol. 51, No. 4, April 1968, pp. 176-179.
6. Pfeiffer, J. D., "Internal Pre ssures in a Wound Roll of Paper," Tappi Journal, Vol. 49, No. 8, August 1966, pp. 342-347.
7. Hakiel, Z., "Nonlinear Model for Wound Roll Stresses," Tappi Journal, Vol. 70, No. 5, May 1980, pp. 113-117.

8. Cole A. K., and Hakiel Z., "A Nonlinear Wound Roll Stress Model Accounting for Widthwise Web Thickness Nonuniformities," ASME, Applied Mechanics Division, Vol. 149, 1992.
9. Kedl D. M., "Using A Two-Dimensional Winding Model to Predict Wound Roll Stresses that Occur Due to Circumferential Steps in Core Diameter or to Cross-Web Caliper Variation," Proceedings of the First International Conference on Web Handling, 1991, pp. 99-112.
10. Lee Y. M., and Wickert, J. A. "Stress Field in Finite Width Axisymmetric Wound Rolls," Transactions of ASME, Journal of Applied Mechanics, Vol. 69, March 2002, pp. 130-138.
11. Mollamahmutoglu, C., and Good, J. K., "Analysis of Large Deformation Wound Roll Models," Transactions of ASME, Journal of Applied Mechanics, Vol. 80, No. 4, p. 041016.
12. Good, J. K., and Pfeiffer, J. D., "Tension Losses During Centerwinding," Proceedings of the 1992 Tappi Finishing and Converting Conference, pp. 297-306.
13. Arola, K., and von Hertzen, R., "Two Dimensional Axisymmetric Winding Model for Finite Deformation," Computational Mechanics, Vol. 40, 2007, pp. 933-947.
14. Good J. K., Wu, Z., and Fikes, M. W. R., "The Internal Stresses in Wound Rolls with the Presence of a Nip Roller," Transactions of ASME, Journal of Applied Mechanics, Vol. 61, 1992, pp. 182-185.
15. Mollamahmutoglu, C., Bulut, O., Adari, S. and Good, J. K., "The Coupling of Winding Models and Roll Quality Instruments," Proceedings of the Thirteenth International Conference on Web Handling, IWEB 2015, June 5-8, 2015, Oklahoma State University, Stillwater, OK